8. García, J. A., Alvarez, S., Flores, A., Govezensky, T., Bobadilla, J. R. and José, M. V., Statistical analysis of the distribution of amino acids in *Borrelia burgdorferi* genome under different genetic codes. *Physica A*, 2004, **342**, 288–293.
9. Holste, D., Grosse, I., Beirer, S., Schieg, P. and Herzel, H., Repeats and correlations in human DNA sequences. *Phys. Rev. E*, 2003, **67**, 061913.
10. Li, C. and Wang, J., Relative entropy of DNA and its application. *Physica A*, 2005, **347**, 465–471.
11. Li, M., Badger, J. H., Chen, X., Kwong, S., Kearney, P. and Zhang, H., An information-based sequence distance and its application to whole mitochondrial genome phylogeny. *Bioinformatics*, 2001, **17**, 149–154.
12. Schneider, T. D., Stormo, G. D., Gold, L. and Ehrenfeucht, A., Information content of binding sites on nucleotide sequences. *J. Mol. Biol.*, 1986, **188**, 415–431.
13. Nandy, A., Investigations on evolutionary changes in base distributions in gene sequences. *Internet J. Mol. Design*, 2002, **1**, 545–548.
14. Blaisdell, B. E., A measure of the similarity of sets of sequences not requiring sequence alignment. *Proc. Natl. Acad. Sci. USA*, 1986, **83**, 5155–5159.
15. Blaisdell, B. E., Average values of dissimilarity measure not requiring sequence alignment are twice the averages of conventional mismatch counts requiring sequence alignment for a computer-generated model system. *J. Mol. Evol.*, 1989, **29**, 538–547.
16. Blaisdell, B. E., Effectiveness of measures requiring and not requiring prior sequence alignment for estimating the dissimilarity of natural sequences. *J. Mol. Evol.*, 1989, **29**, 526–537.
17. Almeida, J. S. and Vinga, S., Alignment-free sequence comparison – a review. *Bioinformatics*, 2003, **19**, 513–523.
18. Qi, J., Luo, H. and Hao, B., CVTree: a phylogenetic tree construction tool based on whole genomes. *Nucleic Acids Res.*, 2004, **32**, W45–W47.
19. Qi, J., Wang, B. and Hao, B., Whole proteome prokaryote phylogeny without sequence alignment: a K-string composition approach. *J. Mol. Evol.*, 2004, **58**, 1–11.
20. Chu, K. H., Qi, J., You, Z. and Anh, V., Origin and phylogeny of chloroplast revealed by a simple correlation analysis of complete genomes. *Mol. Biol. Evol.*, 2004, **21**, 200–206.
21. Basak, S. C., Information theoretic indices of neighborhood complexity and their applications. In *Topological Indices and Related Descriptors in QSAR and QSPR* (eds Devillers, J. and Balaban, A. T.), Gordon and Breach Science, The Netherlands, 1999, pp. 563–593.
22. Nandy, A., Harle, M. and Basak, S. C., Mathematical descriptors of DNA sequences: development and applications. *ARKIVOC*, 2006, **ix**, 211–238.
23. Zupan, J. and Randić, M., Algorithm for coding DNA sequences into 'spectrum-like' and 'zigzag' representations. *J. Chem. Inf. Model.*, 2005, **45**, 309–313.
24. Ghosh, A., Nandy, A., Nandy, P., Gute, B. D. and Subhash Basak S. C., Computational study of dispersion and extent of mutated and duplicated sequences of the H5N1 influenza neuraminidase over the period 1997–2008. *J. Chem. Inf. Model.*, 2009, **49**, 2627–2638.

ACKNOWLEDGEMENTS. R.N. thanks the Department of Science and Technology, New Delhi, India, for financial assistance (No. SR/S4/MS: 479/07). We also thank Mr T. M. Anbazhagan, Inflexion Technology, Bangalore, for his help in developing the computer program.

Received 25 March 2009; revised accepted 21 June 2010

Platinum group elements in basic and ultrabasic rocks around Madawara, Bundelkhand Massif, Central India

S. P. Singh[1,*], V. Balaram[2], M. Satyanarayanan[2], K. V. Anjaiah[2] and Aditya Kharia[1]

[1]Department of Geology, Bundelkhand University, Jhansi 284 001, India
[2]National Geophysical Research Institute (CSIR), Uppal Road, Hyderabad 500 007, India

The southern part of the Bundelkhand Massif shows a series of lensoidal bodies of undeformed and unmetamorphosed ultramafics, associated with gabbro/diorite and intrusive into the Bundelkhand Gneissic Complex (BnGC). The ultramafics exposed around Madawara town is characterized by high MgO (26–46 wt%), and low SiO_2 (42–46 wt%), TiO_2 (< 1 wt%) and Al_2O_3 (< 1 wt%). The concentrations of Cr and Ni are high, ranging from 3000 to 6000 ppm and 1500 to 4000 ppm respectively. Geochemical studies of platinum group elements (PGEs) in fertile ultramafic magma developed at great depths showed depleted to undepleted and undersaturated to saturated conditions around Madawara. The rare earth elements patterns show three distinct trends, viz. strongly depleted Eu anomaly, Eu positive and a flat trend. The high values of ΣPGE (~ 700 ppb) especially Ir PGE (IPGE) and Pt (> 100 ppb) suggest that the Madawara ultramafic complex could be a potential PGE prospect. Detailed exploration studies including bore hole drilling should be taken up.

Keywords: Depletion, fertile mantle, fractionation, partial melting, platinum group elements prospect.

THE platinum group of elements (PGEs) (Ru, Rh, Pd, Os, Ir and Pt) is strongly siderophile and chalcophile in character and is a sensitive indicator of partial melting, crystal fractionation and S-saturation conditions of magma[1–3]. PGEs are an economically important group of elements and there are only few localities with PGE deposits in the world, viz. Norilsk–Talnakh in USSR; Stillwater Complex in USA; Bushveld Complex in South Africa, and Sudbury structure and its associated sulphide deposits in Canada[1,4–8]. It has been suggested that sulphur-saturated melts may have relatively high PGE, especially the Pd group of elements[9], but the possibility of PGE deposits in the sulphur undersaturated conditions cannot be ignored[4]. The latter view is mainly related to the oxide facies, which contains high platinum. The oxide facies appears in most of the magma before the appearance of the sulphide facies minerals. High values of PGE have been reported from many mafic and ultramafic terrains of dif-

*For correspondence. (e-mail: spsinghbu@rediffmail.com)

ferent tectonic settings but PGE mineralization are mainly associated with layered intrusions, komatiites and ophiolits suites[1,10]. In India, the PGE mineralized zones have been identified from ultramafics of Nausahi, Orissa[8], Hanumalapur, Karnataka[11] and Karungalpatti, Tamil Nadu.

Occurrences of ultramafic rocks were known around Madawara since the last few decades[12–14], but no attempt has been made to understand the PGE mineralization in these rocks mainly due to non-availability of analytical facilities. High concentration of PGE has been reported from the ultramafics of Ikauna, Lalitpur since the last two years only in the form of reports abstracts[15]. The present data reveal that ultramafic rocks of Madawara town have a potential for PGE mineralization.

The Bundelkhand Massif consists of a variety of granitoids of Palaeoproterozoic age on a large scale (> 60% of the area of massif) and lensoidal occurrences of low-grade and high-grade metamorphics[13,14,16]. Recent work[17] on Bundelkhand Craton proposed several tectonothermal events (Table 1) and suggested that high-grade supracrustal rocks (proposed as Bundelkhand Gneissic Complex (BnGC: M_2 event), were evolved in the middle Archean time. It was followed by volcano-sedimentary sequences which were less deformed and metamorphosed (low grade) in subsequent events (proposed as Bundelkhand Metasedimentary and Metavolcanics (BMM): M_2). The presence of xenolithic outcrops and intrusive relationships of nearly undeformed Bundelkhand granitoids (BG) limits the above events.

The occurrences of mafic and ultramafics as enclave in the BG have also been described by many workers[12–14,17] from different locations. However, its position in the stratigraphic order of Bundelkhand Craton was uncertain, mainly due to lack of information about field relationships, structural, petrological and geochronological data. The ultramafics of Bundelkhand Massif has been classified into two groups[18], viz. mafics and ultramafics associated with the volcano-sedimentary sequences having close relationship with BMM confined to central part; and ultramafics associated with gabbro and diorite in the granite–gneissic terrain around Madawara as Madawara ultramafics complex or Madawara Igneous Complex (MIC) (Table 1).

The geological study around Madawara (Figure 1) shows several outcrops of mafic and ultramafic rocks into the granite–gneisses of BnGC, which are associated with diorite/gabbro rocks. The ultramafic body trending in E–W direction has a sheared relationship with rocks of BnGC (migmatites, granite–gneisses, gneisses) at both its ends, i.e. near Madawara fort and near the mosque in the northern part, and in the Rohini River near the dam in the southern part. The sheared zone is about 40–50 m thick, where ultramafics are found to transport southwards.

The rocks of BnGC and BMM of Madawara area are also dominated by E–W trend and overlaid by sedimentary cover of Bijawar Group and Vindhyan Supergroup in the southern part at Sonrai, about 8 km south of the study area. Several NW–SE trending shear fractures/faults have been observed to displace the ultramafics, BMM, Bijawar and BnGC rocks.

The MIC is about 40 km in length and 2–4 km wide zone of mafic, ultramafic, diorite/gabbro magmatism, where rocks are mostly dominated by mafic–ultramafic suite of several episodes followed by late phase intrusive of gabbro/diorite associations. The Palaeoproterozoic BG were also found to be intrusive into gneisses of BnGC and MIC which indicates that mafic and ultramafic emplacement would be pre-BG (> 2600 Ma). The northern and southern contacts of E–W trending MIC rocks are sheared and mylonitized, where ultramafics along with BnGC are involved in shearing. The mafic and ultramafics of Madawara are mostly dark bluish grey coloured, coarse-grained and massive in nature. The medium to coarse grained spinel embedded into the peridotite are visible at several places (Figure 2). The layered structures were also noted at few places especially to the south of Madawara town. Globular structures (Figure 2 *c*) (marked as rounded blebs) of ultramafics in the light grey pyroxenite were found commonly in the southern part of the area (near sample MD 20) which may be an indication of

Table 1. Stratigraphy of Bundelkhand Craton

Vindhyan Supergroup (1400–700 Ma)	Lower Vindhyan limestones and dolomites, quartzite, upper Vindhyan Kaimure sandstone, Rewa sandstone and shales, Bhander carbonates
Bijawar/Gwalior Group (1800–1600 Ma)	Sandstones, quartzites, micacious quartzite, meta basics, ferruginous shale and sands stones, BHJ, limestones and dolomites
Mafic emplacement (2000–1800 Ma)	Dolerites, gabbro, lamproites, quartz veins and reefs, granites
Late phase granitic emplacement (2300–2000 Ma)	Quartz reef, granitoids, pegmatites, diaspore and pyrophyllites
Bundelkhand granitoids (BG) (2600–2500 Ma)	Leucogranite, biotite granite, hornblende granite, hornblende–biotite granite
Madawara Ultramafics Complex	Peridotite, dunnite, hartzbugite, spinel bearing peridotite, PGE enriched peridotites, pyroxenite, gabbro, diorite, quartz diorite, granite, talc chlorite, schist, etc.
Bundelkhand metasedimentaries and metavolcanics (3300–2600 Ma)	BMQ, rhyolite, andesite, rhyodacite, quartzite, micaceous quartzite, chlorite schist, talc schist, pyroxenite, gabbro, peridotite, calc-schist
Bundelkhand Gneissic Complex (> 3300 Ma)	Granite–gneisses, calc silicate, gneisses, quartzites, garnetiferous gneiss, sillimanite–cordierite gneiss, amphibolite, TTG

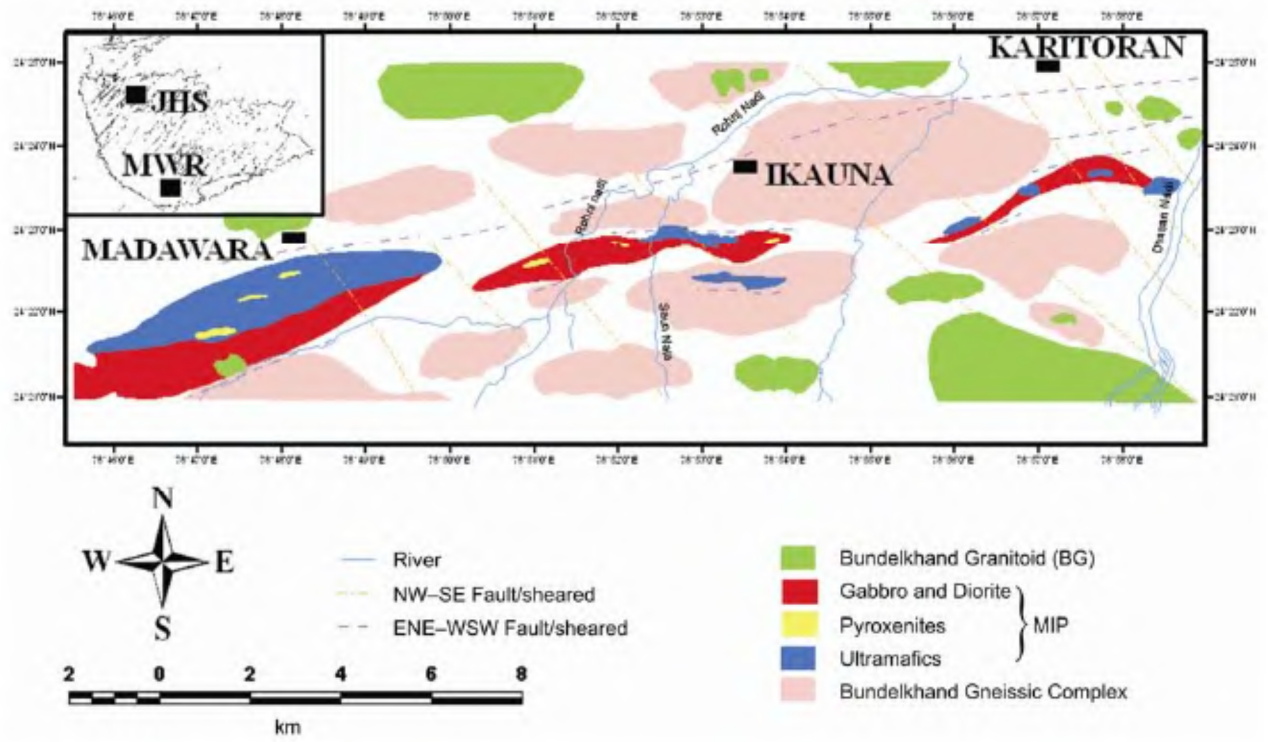

Figure 1. Geological map of Madawara Igneous Complex, Bundelkhand Craton. (JHS: Jhansi; MWR: Madawara.)

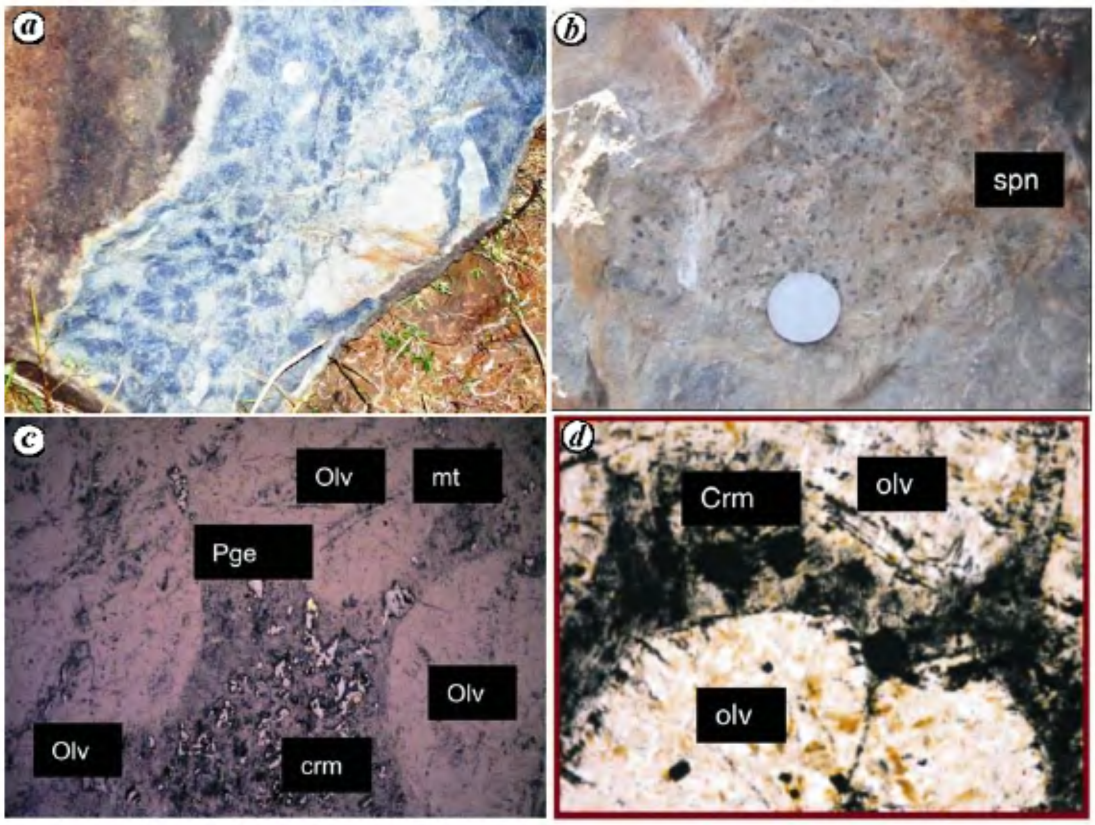

Figure 2. ***a***, Fieldgraph showing globular texture from the ultramafics an indication of two varieties of magmic components. The dark variety consists of high values of platinum group elements (PGE); ***b***, Field photograph showing crystals of spinel embedded in ultramafics; ***c***, Photomicrograph showing the sulphide minerals (Pge), magnetite pyrrhotite (mt) and chromites (crm) present as disseminated crystals in the intergranular spaces of cumulates of olivine (Olv); ***d***, Growth of cpx and chromite mineral (Crm) in the interstitial spaces of olivine (olv) cumulates.

the fractionation of two ultramafic components. In most of the places, the ultramafics are highly altered, serpentinized and chloritized. Sometimes, the disseminated specks of sulphide minerals especially in highly dark coloured ultramafics are also visible at several places. The sulphide-rich ultramafic layers were encountered near the pyroxenites, showing some kind of layered structure in the ultramafics. The stringers and veinlet structures were also observed in the ultramafics related to subsequent emplacement of PGE enriched ore fluid and magmatic body in the fractured zones. The pyroxenite and peridotite intrusive (late phase) in MIC are less altered and nearly undeformed to dunite, peridotite, harzburgite, websterite spinel-bearing peridotite that are deformed, locally mylonitized and serpentinized and sometimes changed into talc ± chlorite ± magnetite/chromites ± actinolite ± tremolite schists.

Petrographic studies suggest presence of cumulates of olivine in the ultramafics. Most of the olivine and pyroxene are altered into chlorite and talc. Unaltered olivine and pyroxene are very rare and if present they are usually zoned. Medium to coarse-grained crystals of hercynite/chromite are mainly confined to the rim part of olivine whereas the core part of olivine is devoid of inclusion. The crystals of orthopyroxene usually contain medium-grained granules of magnetite along their cleavages. Sulphide and iron oxides are mostly embedded in the ground mass of cumulates of olivine (Figure 2) and sometimes in the interspaces of olivine and pyroxene cumulates. The pyroxenes are usually zoned and their core part normally enriched with iron oxides. The sulphide phases are usually disseminated and found along the opening of cleavages or fracture zone or in the interstitial spaces of olivine cumulates. The platinum group of minerals are present in the disseminated form especially in the matrix of olivine cumulates (Figure 2). Amphibole and chlorite are the most dominating altered minerals in the ultramafics. Actinolite and tremolite crystals are also common in the altered rocks and sometimes define the foliation developed due to mylonitization and subsequent thermal effects. Hornblende crystal is mostly found in the pyroxenite, diorite, granite and intrusive peridotite. Magnetite is abundant in minerals; occurs as primary and secondary phases, both along the cleavages of olivine, pyroxenes, talc and tremolite. Fine-grained granular aggregate of magnetite is found in cliopyroxene as primary crystals whereas that of coarse grained is found with talc–chlorite–serpentine minerals as secondary crystals.

Representative samples of peridotites and pyroxenites were collected so as to avoid vein fillings and alteration rinds, cleaned and then powdered using an agate mortar. Major oxides (SiO_2, TiO_2, Al_2O_3, Fe_2O_3, MnO, MgO, CaO, Na_2O, K_2O and P_2O_5) were determined in all the ultramafic samples by X-ray fluorescence (XRF) (Philips MagiXPRO-PW2440) at the National Geophysical Research Institute (NGRI), Hyderabad, India. International geochemical standard reference materials (SRMs) from the US Geological Survey, Canadian Geological Survey, International Working Group, France and NGRI, India were used to prepare calibration curves for major oxides. Trace rare earth elements (REE) and PGE were determined by ICP–MS (PerkinElmer SCIEX ELAN® DRC-II) at NGRI, Hyderabad. Analyses of PGE and Au were carried out by following NiS–fire assay with Te co-precipitation and ICP–MS methods. Single isotopes were used for all elements and were selected based on their abundance levels and freedom from interferences from other elements usually present in rock samples. The detection limits of most of the elements including PGE were about 0.01 ng/ml, and the precision was better than 6% for trace and REE, and < 10% for PGE analysis[19,20].

The major oxides and trace element compositions of representative ultramafics and mafics (olivine-bearing websterite, harzburgite, gabbro and orthopyroxenite) are listed in Table 2. The olivine websterite at MIC have SiO_2 ranging from 44.2 to 51.0 wt%, Al_2O_3 from 0.9 to 1.0 wt%, CaO from 1.4 to 7.3 wt% and TiO_2 from 0.5 to 0.9 wt%. The harzburgite have SiO_2 ranging from 42.3 to 45.7 wt%, Al_2O_3 from 0.8 to 0.9 wt%, CaO from 0.1 to 2.6 wt% and TiO_2 from 0.3 to 0.7 wt%. The orthopyroxenites have SiO_2 ranging from 44.5 to 50.9 wt%, Al_2O_3 from 0.7 to 0.9 wt%, CaO from 0.1 to 1.6 wt% and TiO_2 from 0.1 to 0.5 wt%. Thus, these rocks are ultrabasic in compositions. All the samples have MgO ranging from 26.4 to 35.9 wt% with Mg# from 83 to 88 and almost linear inverse patterns have been obtained with SiO_2 (Figure 3 *a*). Their Na_2O contents are generally between 0.01 and 0.11 wt%, much higher than K_2O (max 0.04 wt%). The basic rocks of Madawara associated with ultramafic are rich in CaO and poor in Fe_2O_3 and MgO, and differ in many respects from the ultramafics.

The olivine-bearing, websterite and harzburgite have similar chondrite normalized REE patterns slightly enriched in LREE (light REE) (Figure 4 *a*) and display prominent negative Eu anomaly (Eu/Eu* = 0.16–0.91). Their plots in a primitive mantle normalized incompatible element spider diagram are enriched in large ion lithophile elements (LILE) such as Rb, Ba and Th, and depleted in high-field strength elements (HFSE) such as Nb. These rocks have low Eu, Sm and Nd and their $(La/Gd)_N$ ratios range from 0.87 to 1.35, $(La/Yb)_N$ from 1.1 to 1.8 and $(Gd/Yb)_N$ ratios range from 1.09 to 1.47. The ultramafics have overall V-shaped patterns in the chondrite-normalized diagrams and are komatiite to basaltic komatiite in composition. The elemental distribution of different rocks across the strike (E–W) yield more or less a flat trend for major oxides MgO, FeO, Al_2O_3 from the ultramafics. The periodotites that are intrusive into the ultrabasics (phase I) are slightly enriched in the LILE and LREE and nearly flat in MREE (Figure 4 *a*). The gabbro and diorite rocks that are associated with ultramafics show two varieties of trends, i.e. Eu positive and Eu

Table 2. Analytical data of ultramafic rocks from Madawara Igneous Province Complex

Sample	MD-2	MD-3	MD-4	MD20	MD-6	MD-8	MD-9	MD-12	MD26	MD27
SiO_2	44.75	43.68	42.84	43.75	45.30	44.47	50.49	46.92	50.15	49.28
Al_2O_3	0.93	0.84	0.89	0.84	0.91	0.73	0.96	1.00	12.41	14.22
Fe_2O_3	12.86	12.94	14.45	13.79	13.65	14.05	10.27	13.60	13.27	13.44
MnO	0.13	0.14	0.14	0.14	0.15	0.10	0.14	0.14	0.13	0.12
MgO	33.91	34.18	34.26	35.20	32.27	34.45	26.40	29.98	13.11	12.64
CaO	2.60	1.45	1.37	0.08	2.51	0.08	7.26	3.59	13.02	12.65
Na_2O	0.06	0.01	0.02	0.01	0.03	0.02	0.05	0.07	1.52	1.45
K_2O	0.02	0.01	0.01	0.01	0.01	0.00	0.04	0.02	0.31	0.86
TiO_2	0.66	0.49	0.49	0.56	0.51	0.10	0.62	0.90	0.29	0.28
P_2O_5	0.03	0.02	0.02	0.03	0.02	0.01	0.02	0.04	0.04	0.04
LOI	4.88	7.05	5.53	6.01	5.39	6.87	2.65	4.21	0.79	1.04
Sc	14.93	11.39	11.96	12.53	14.08	7.14	19.68	16.57	26.27	30.87
V	110.35	72.28	90.30	83.35	98.52	27.83	115.88	139.05	161.29	135.25
Cr	4650.72	4525.60	5616.48	4843.01	4589.37	2540.42	3450.85	4453.61	429.13	650.13
Co	101.90	118.84	117.84	125.83	85.50	168.30	79.82	98.64	40.18	38.68
Ni	1581.33	1937.51	1852.43	1819.48	1426.26	2063.48	1319.79	1357.92	264.39	224.01
Cu	26.09	22.29	39.32	29.16	22.25	62.73	64.55	38.08	137.74	123.27
Zn	57.26	45.34	70.70	59.14	57.33	52.41	31.37	52.00	28.15	44.89
Ga	5.88	3.93	4.79	4.13	5.09	1.34	5.28	7.57	14.78	12.34
Rb	1.76	0.69	0.95	0.82	1.09	0.70	2.52	0.92	10.40	10.66
Sr	20.32	16.91	16.07	4.79	13.33	8.51	23.26	27.20	167.56	169.14
Y	4.57	3.24	4.00	3.20	4.19	1.00	4.22	6.85	6.68	7.49
Zr	12.25	8.74	7.59	11.27	8.71	1.52	10.61	19.94	11.07	17.96
Nb	0.46	0.38	0.31	0.37	0.39	0.12	0.37	0.62	0.40	0.71
Cs	0.22	0.10	0.14	0.10	0.15	0.06	0.35	0.16	0.25	0.24
Ba	39.31	13.06	14.80	14.64	13.23	17.07	13.41	83.92	55.05	70.92
La	0.85	0.63	0.79	0.80	0.80	0.50	0.87	1.31	1.28	3.40
Ce	3.21	2.44	2.81	2.91	2.98	1.42	3.49	4.98	4.43	5.71
Pr	0.47	0.34	0.38	0.38	0.47	0.18	0.48	0.67	0.60	0.63
Nd	2.14	1.55	1.76	1.73	2.14	0.76	2.18	3.11	2.75	3.15
Sm	0.60	0.45	0.53	0.47	0.56	0.17	0.54	0.86	0.83	0.81
Eu	0.13	0.10	0.09	0.03	0.16	0.08	0.19	0.24	0.32	0.34
Gd	0.76	0.59	0.65	0.57	0.73	0.22	0.74	1.13	1.10	0.90
Tb	0.13	0.09	0.11	0.10	0.12	0.03	0.11	0.18	0.17	0.16
Dy	0.77	0.56	0.66	0.56	0.74	0.16	0.69	1.14	1.12	1.13
Ho	0.17	0.12	0.14	0.13	0.16	0.03	0.16	0.25	0.25	0.24
Er	0.52	0.37	0.44	0.40	0.52	0.09	0.51	0.78	0.76	0.64
Tm	0.09	0.06	0.07	0.06	0.09	0.02	0.08	0.13	0.12	0.08
Yb	0.49	0.34	0.43	0.39	0.50	0.09	0.48	0.72	0.73	0.48
Lu	0.09	0.06	0.07	0.06	0.08	0.01	0.08	0.13	0.12	0.09
Hf	0.24	0.17	0.15	0.22	0.19	0.04	0.22	0.41	0.25	0.50
Ta	0.04	0.11	0.06	0.03	0.08	0.03	0.05	0.05	0.03	0.05
Pb	14.83	10.58	11.10	9.80	7.60	10.64	12.13	11.75	4.57	2.98
Th	0.27	0.18	0.18	0.25	0.25	0.06	0.21	0.33	0.24	0.58
U	0.19	0.11	0.13	0.19	0.10	0.18	0.14	0.19	0.12	0.11
Ru	64.6	57.8	79.2	77.6	74.2	100.2	64.8	82		
Rh	6.2	17.6	15	6.8	9.8	2.4	8.6	9.6		
Pd	15.6	76.4	30.6	37.4	33	17	172.2	87.2		
Os	7.2	12	15	6.8	13	7.6	1.8	11.6		
Ir	18.8	18.2	13.6	17.6	20	9.4	5.4	12.2		
Pt	30.6	71	34.6	276.6	43.6	131.6	100	82.8		
Au	32	262.8	36.2	54.6	32	42.2	38	53.6		
∑PGE	143	253	188	422.8	193.6	268.2	352.8	285.4		

negative with the flat REE (Figure 4 *a*). Thus the REE diagrams suggest multiphase magmatism in the MIC.

PGE contents of the mafic and ultramafics at MIC presented in Table 2 display a unique trend, i.e. low in Pd and high in Pt and Au (Figure 4 *b*). The PGE geochemical trend points out that the ultramafics of Madawara is a potential zone for Cr, Ni and PGE mineralization. These ultramafics have almost a narrow range of PGE. The high values of Ir and Ru contents varying from 5.4 to 20 ng/g and 57.8 to 100.2 ng/g respectively. Rh contents are fairly constant with a range of 2.4 to 17.6 ng/g, whereas Pt contents vary from 30.6 to 276.2 ng/g and Pd from 17

to 172 ng/g. Au also displays wide variation ranging from 32 to 262 ng/g. Pd/Ir ratios range from 0.52 to 5.14, whereas Pd/Pt ratios vary between 0.11 and 1.0 in the ultramafic of MIC. Mg#s exhibits feeble positive correlation with Ru, Rh, Os, Ir and Pt, but shows no correlation with Pd. It shows slightly negative correlation with Au.

The three major processes for the origin of PGE fractionation have been discussed, viz. partial melt, crystal/liquid sulphide fractionation, and alteration. Of all these factors, degree of partial melting is the major controlling factor for the PGE concentration[21,22]. Besides this, degree of dissolved sulphur, time of S-saturation, shape and size of magma chamber and tectonic environment are also important factors[6]. It is established that IPGE (Ir, Os, Rh) and PPGE (Pd, Pt, Ru) are two important divisions in PGE which behave distinctly in several respects for fractionation, sulphidization, crystallization and PGM mineralization[3,7]. The study[3,22,23] reveals that IPGE cannot be retained in olivine and spinel due to its compatibility whereas PPGE prefers the melt phase at an early stage due to incompatibility. It has been observed that sulphides enclosed in the silicate phase usually have high Os and Ir abundance and low Pd/Ir ratios[24], whereas the pentlandite dominated interstitial sulphides can show low Os and Ir and high Pd/Ir ratios[7]. Silicate hosted sulphides are considered as the residue of partial melting of magma at high temperature, whereas interstitial sulphides are the crystallization product of sulphides bearing melt that developed at relatively low melting points[9]. Thus under a low degree of partial melting, the interstitial sulphides are preferentially incorporated into the liquid phase that produces a PPGE rich melt with high Pd/Ir ratio[1,25,26], whereas the IPGE enriched magma developed at high temperature by high degree of partial melting contain low Pd/Ir ratio.

It has been described that at higher temperature, as the degree of partial melting increases, the silicate enclosed sulphides with IPGE melts produces lower Pd/Ir ratio[23]. This view suggests that high Ir involving melt is dependent on the temperature and degree of partial melting. Thus the low Pd/Ir ratio from MIC explains the high degree of partial melting. The high degree of partial melt developed in the sulphur saturated environment is a strong potential zone for PPGE and the sulphur under-saturated magma for IPGE. PGE remains in the primary melt of komatiite with low Pd/Ir developed in the sulphur undersaturated condition and becomes potential as they survived S saturated conditions during the evolution.

PGE concentration also is controlled by the dissolved sulphur content and time of the solidification of sulphur-bearing phases. The dissolved sulphur plays an important role in PGE mineralization due to strong siderophilic character of PGE in the magma chamber or during cooling.

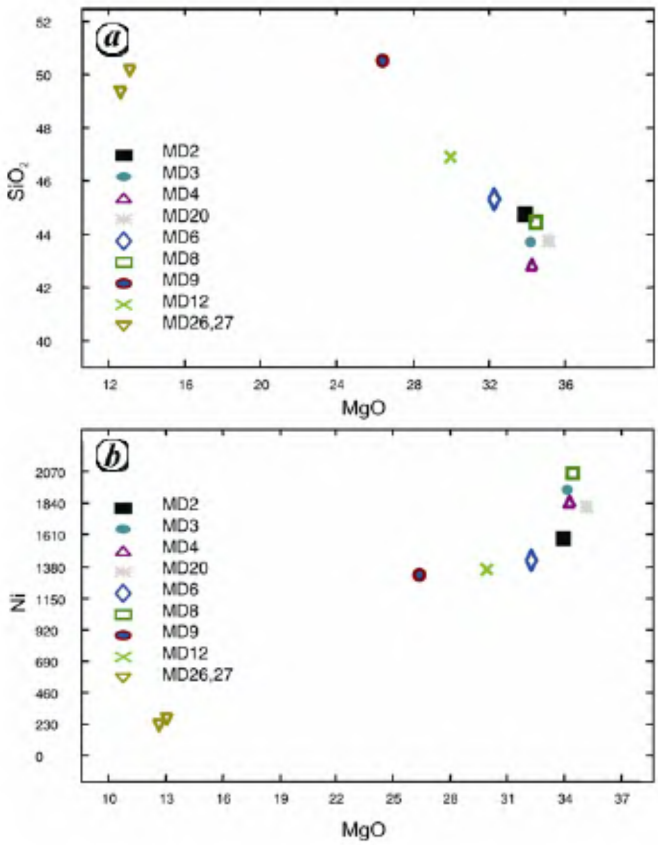

Figure 3. MgO relationship with SiO_2 (*a*) and Ni (*b*) in Madawara ultramafic rocks.

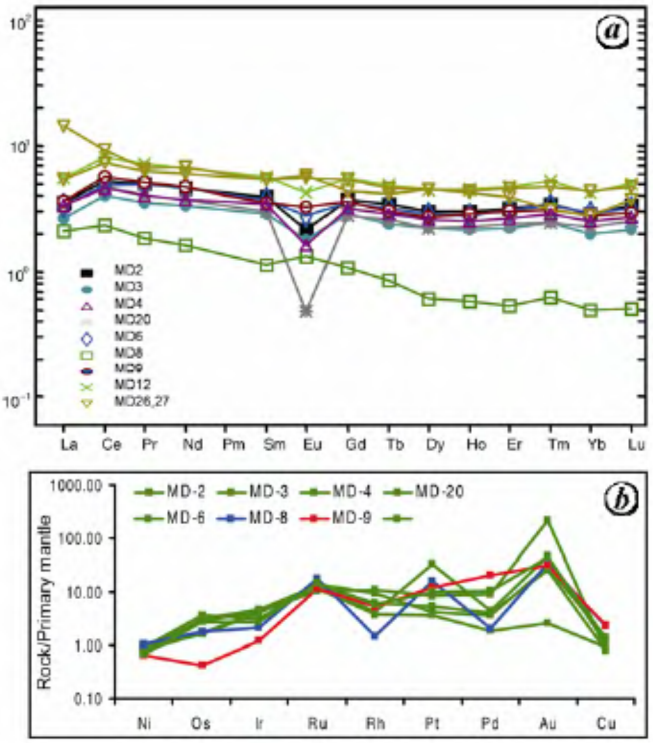

Figure 4. *a*, Chondrite-normalized rare earth elements patterns of ultramafic rocks of Madawara; *b*, PGE trend for the ultramafics of Madawara showing the Pt and Au enriched trend.

It is found that PGE and other chalcophile elements in the mafic and ultramafics rocks are mainly controlled by the amount of dissolved sulphur in the magma chamber. The genetic models for the PGE-bearing ore bodies invoke separation of the immiscible sulphide liquid magma and its fractionation and an accumulation on the floors of magma chambers by various workers[6,25,28].

In most of the sulphur saturated mineralized cumulates, PGE are mainly associated with sulphides that appear due to fractionation of magma as the immiscible sulphide liquid, whereas in the case of 'S' poor mafic and ultramafic cumulates, the picture is more complicated. PGE including the relative proportion may be trapped into the intercumulus liquid in the presence or absence of cumulus sulphide and chromite[4,5,11].

The proportion of PGE, Ni and Cu in the mafic and ultramafic magma is mainly controlled by the distribution of sulphides, chromite, olivine and PGM[9,29]. Because of the strong siderophilic character and high degree of distribution coefficient constant, the crystallization of PGM is much faster than Ni and Cu sulphides[1]. The geochemical data along with textural study (Figure 2) of Madawara reveals that the first phase of formation was strongly enriched with PGE under the moderate to low 'S' saturation conditions (Figure 5) and was komatiitic in character (Figure 6). This is also evident from the discrimination diagram proposed by Barnes[9] (Figure 7). In subsequent stages of magmatic fractionation due to increase in the sulphide, PGE were scavenged by the sulphur much faster than Ni, Cu and Fe; that has been responsible for the development of different sulphide phases of PGE mineralization in the periodotite intrusive of Madawara ultramafics. The abnormally high values of Pt and other

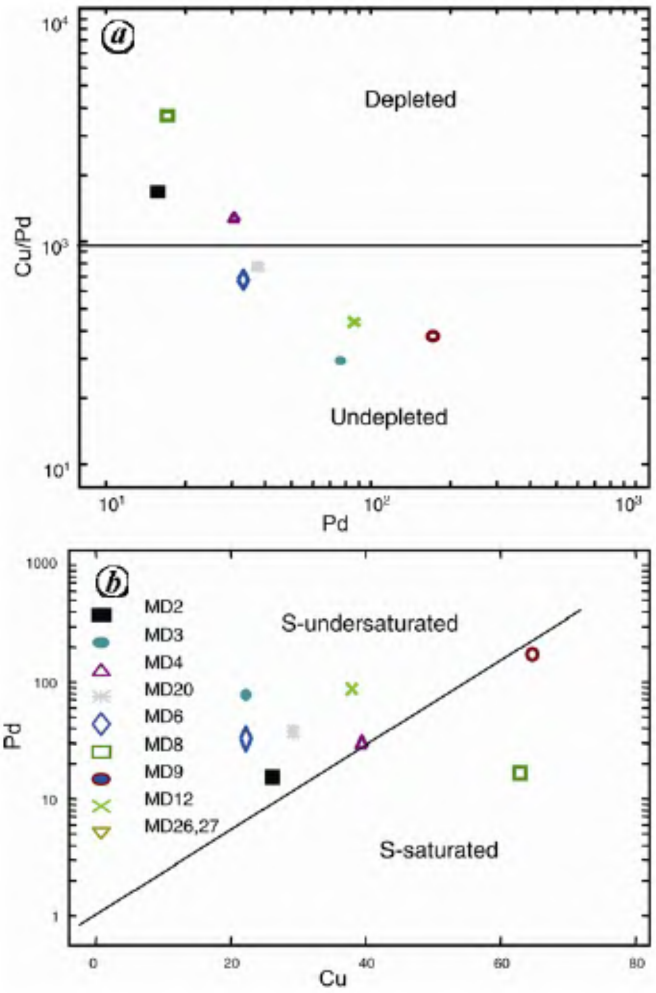

Figure 5. Plot of Cu versus Pd and Cu/Pd vs Pd for ultramafic rocks from Madawara ultramafics indicating its undepleted to depleted nature.

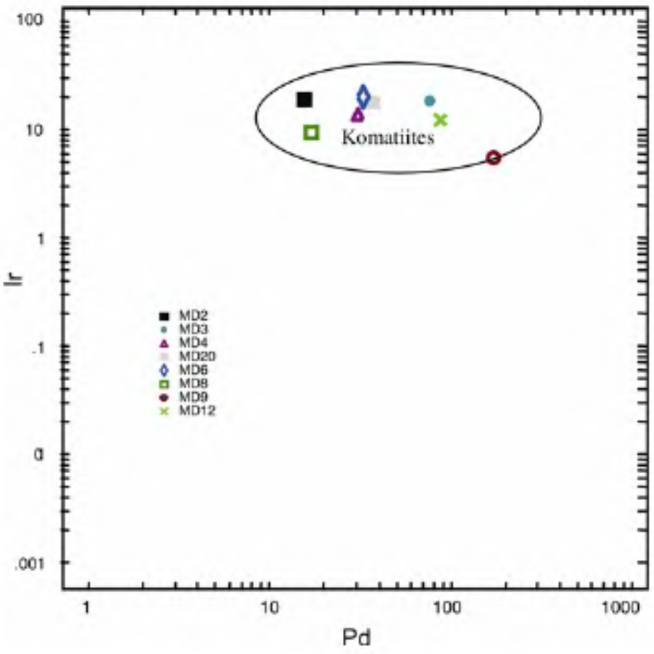

Figure 6. Pd versus Ir diagram of ultramafic rocks from Madawara ultramafics.

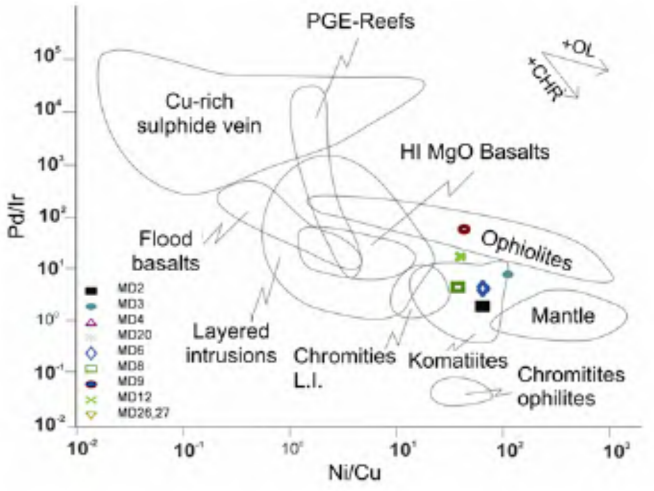

Figure 7. Discrimination diagram showing Ni/Cu versus Pd/Ir in ultramafic rocks from MIC.

PGE from several samples and presence of sulphidization signatures support this view. It is suggested that Pd could be concentrated in the pentlandite whereas Ir is evenly distributed among chromite, pentlandite and pyrrhotite[30]. Pd/Ir ratio varied from 1 to 7.0 exceptionally high up to 32 in some ultramafics. The relatively uniformly constant Pd/Ir ratio in the ultramafics is an indication of the complete separation of sulphide phases from the silicate magma and leaving behind the silicate magma which is devoid of sulphide minerals[31]. The variable of Pd/Ir ratio from ultramafic of Madawara indicates that 'sulphur' saturated to undersaturated conditions prevailed (Figure 5). In the initial stage of magmatic evolution, Ir migrates to the base of sulphide and fractionates sulphide depleted melt in IPGE and subsequently enriched PPGE in the melt.

The S and Cu are sensitive during the magmatic differentiation. Therefore, Cu/Pd, Cu/Ir, Ni/Pd have been used as suitable analogues for sulphur discrimination, especially when the loss of 'sulphur' from the magma system is suspected[29,32,33]. In the S-undersaturated melts, Cu/Pd, Ni/Pd and Cu/Ir ratios have a narrow range for ultramafic Madawara. The scattered values in variation diagram Pd versus Cu indicate saturated to undersaturated conditions of sulphur prevailed in the ultramafics of Madawara (Figure 5 *a*). The plots also reveal that early phase magmatism occurred during undersaturated conditions. The distinct trend of PGE crystallization from the discrimination diagram Ni/Pd versus Cu/Ir and Cu/Pd versus Pd suggests that sulphur activity increases in the late stage of magmatism in Madawara (Figure 5 *b*).

Four types of PGE mineralization: silicate hosted Pd type; silicate hosted Pt type; base metals sulphide Pd type, and oxide hosted PGE type deposits have been described from Hanumalpur area of Karnataka[11]. MIC consists of high volumes Ir, Ru, Pt, Au and Ag along with high concentration of Ni, Co and MgO and low values of V, Ti, Pd and Cr. The ultramafics of MIC are devoid of nickel and chromite layers. Chromite is only present in disseminated form in the matrix of silicates or sometimes as medium to coarse-grained disseminated grains in the pyroxene. Therefore, PGE mineralization for Madawara may be related to second, third and fourth categories. The positive correlations between Ir, Pd and Ni of Madawara ultramafics and intergranular spaces of olivine cumulate filled by chromite, magnetite and pyrhotite (Figure 2) suggest the presence of nickel sulphides and pyrrhotites[34]. Similar conditions have been described for PGE mineralization from komatiites rocks of other places[1,22,34]. The REE and PGE patterns, trace element ratios of PGE contents and Pd/Ir ratios of Madawara are comparable to those of a rock layered intrusive to komatiite[35]. The plot of geochemical data, textural studies and Ni/Cu versus Pd/Ir discrimination (Figure 7) diagram clearly indicates that ultramafic of Madawara represents fertile magma and the area may be a strong potential zone for PGE mineralization. Detailed exploration studies have to be taken up.

The genesis of mineralization is somewhat unclear at this stage of study, especially because of mylonitization of ultramafics rocks at both their ends, but the evidence gathered so far suggests a complex model involving multiphase magmatism and sulphidation responsible for sulphide phase fractionation of PGE and mineralization in the lensoidal forms.

1. Barnes, S. J., Naldrett, A. J. and Gorton, M. P., The origin of the fractionation of the platinum-group elements in terrestrial magmas. *Chem. Geol.*, 1985, **53**, 303–323.
2. Barnes, S. J., The use of metal ratios in prospecting for platinum group elements deposits in mafic and ultramafics intrusions. *J. Geochem. Expln.*, 1990, **37**, 91–99.
3. Chen, G. and Xia, B., Platinum-group elemental geochemistry of mafic and ultramafic rocks from the Xigaze ophiolite, southern Tibet. *J. Asian Earth Sci.*, 2008, **32**, 406–422.
4. Stone, W. E. and Crocket, J. H., Platinum-group element contents of chromites from mafic-ultramafic layered flows, Abitibi greenstone belt, Ontario: implications for geochemical fractionation and mineral exploration. *Mineral. Petrol.*, 2003, **78**, 139–147.
5. Filho, F., Naldrett, A. J. and Gorton, M. P., REE and pyroxene compositional variation across the Niquelândia layered intrusion, Brazil: petrological and metallogenetic implications. *Trans. Inst. Min. Metall.*, 1998, **107**, 1–22.
6. Peach, C. L. and Mathez, E. A., Constraints on the formation of platinum group deposit in igneous rocks. *Econ. Geol.*, 1996, **91**, 430–450.
7. Day, J. M. D., Pearson, D. G. and Hulbert, L., Rhenium–osmium isotope and platinum group element constraints on the origin and evolution of the 1.27 Ga Muskox intrusion. *J. Petrol.*, 2008, **49**, 1255–1295.
8. Mondal, S. K., Robert, F. and Ripley, E. M., Os isotope systematics of mesoarchean chromitite-PGE deposits in the Singhbhum Craton (India): implications for the evolution of lithospheric mantle. *Chem. Geol.*, 2007, **244**, 391–408.
9. Barnes, S. J., The use of metal ratios in prospecting for platinum group element deposits in mafic and ultramafic intrusions. *J. Geochem. Explorn.*, 1990, **37**, 91–99.
10. Balaram, V., Recent advances in the determination of PGE in exploration studies – a review. *J. Geol. Soc.*, 2008, **72**, 661–677.
11. Alapieti, T. T., Devaraju, T. C. and Kaukonen, R. J., PGE mineralization in the late Archaean iron-rich mafic–ultramafic, Hanumalapur Complex, Karnataka, India. *Mineral Petrol.*, 2008, **92**, 99–128.
12. Prakash, R., Swarup, P. and Srivastava, R. N., Geology and mineralization in the southern parts of Bundelkhand in Lalitpur district, Uttar Pradesh. *J. Geol. Soc. India*, 1975, **16**, 143–156.
13. Sharma, R. P., Lithostratigraphy, structure and petrology of the Bundelkhand group. In *Geology of Vindhyanchal* (eds Valdia, K. S., Bhatia, S. B. and Gaur, V. K.), Hindustan Publication, New Delhi, 1982, pp. 30–46.
14. Basu, A. K., Geology of parts of the Bundelkhand granite massif. *Rec. Geol. Surv. India*, 1986, **117**(2), 61–124.
15. Farooqui, S. A. and Singh, A. K., Platinum mineralization in Ikauna Area, Lalitpur District, Uttar Pradesh. *J. Geol. Soc. India*, 2006, **68**, 582–584.
16. Basu, A. K., Role of the Bundelkhand granite massif and the Son–Narmada megafault in Precambrian crustal evolution and tectonism in central and western India. *J. Geol. Soc. India*, 2007, **70**, 745–770.
17. Singh, S. P., Singh, M. M., Srivastava, G. S. and Basu, A. K., Crustal evolution in Bundelkhand area, Central India. *J. Him. Geol.*, 2007, **28**, 79–101.

18. Singh, S. P. and Singh, M. M., Geochemistry of Archean mafic and ultramafics rocks from central part of Bundelkhand craton: implication in the Archean crustal evolution. *J. Ecol. Geol. Georesources Mag.*, 2009, **8**, 1–15.
19. Roy, P., Balaram, V., Anil Kumar, Satyanarayanan, M. and Rao, G., New REE and trace element data on two international kimberlitic reference materials by ICP-MS. *J. Geostand. Geoanal. Res.*, 2007, **31**(3), 261–273.
20. Balaram, V., Mathur, R., Banakar, V. K., James, R. Hein, Rao, C. R. M., Gnaneswara Rao, T. and Dasaram, B., Determination of the platinum-group elements and gold in manganese nodule reference samples by nickel sulphide fire-assay and Te-coprecipitation with ICP-MS. *Indian J. Mar. Sci.*, 2006, **35**(1), 7–16.
21. Crocket, J. H., Platinum-group elements in mafic and ultramafic rocks: a survey. *Can. Mineral*, 1979, **17**, 391–402.
22. Crocket, J. H. and Teruta, Y., Palladium, iridium and gold contents of mafic and ultramafic rocks drilled from the mid-Atlantic ridge, Leg 37, Deep Sea Drilling Project. *Can. J. Earth Sci.*, 1977, **14**, 777–784.
23. Mitchell, R. H. and Keays, R. R., Abundance and distribution of gold, palladium and iridium in some spinel and garnet lherzolites: implications for the nature and origin of precious metal-rich intergranular components in the upper mantle. *Geochim. Cosmochim. Acta*, 1981, **45**, 2425–2442.
24. Alard, O., Griffin, W. L. and Lorand, J. P., Non-chondritic distribution of the highly siderophile elements in mantle sulphides. *Nature*, 2000, **407**, 891–894.
25. Naldrett, A. J., Hoffman, E. L., Green, A. H., Chen, L. C. and Naldrett, S. R., The composition of Ni-sulphide ores, with particular reference to their content of PGE and Au. *Can. Mineral.*, 1979, **17**, 403–415.
26. Naldrett, A. J., Platinum group element deposits. In *Platinum Group Elements – Mineralogy, Geology, Recovery* (ed. Cabri, L. J.), Canadian Institute of Mining, Metallurgy and Petroleum, Special volume 23, 1981, pp. 197–232.
27. Seitz, H. M., Keays, R. R., Platinum group element segregation and mineralization in a noritic ring complex formed in Proterozoic siliceous high magnesium basalt magmas in the Vestfold Hill, Antarctica. *J. Petrol.*, 1997, **38**, 703–725.
28. Campbell, I. H. and Naldrett, A. J., The influence of silicate : sulphide ratios on the geochemistry of magmatic sulphides. *Econ. Geol.*, 1979, **74**, 1503–1505.
29. Barnes, S. J., Boyd, R., Korneliussen, A., Nilsson, L. P., Often, M., Pedersen, R. B. and Robins, B., In *Geo-Platinum* (eds Prichard, H. M. *et al.*), Elsevier, 1988, vol. 87, p. 113.
30. Chyi, L. L. and Crocket, J. H., Partition of platinum, palladium, iridium, and gold among coexisting minerals from the deep ore zone, Strathcona mine, Sudbury, Ontario. *Econ. Geol.*, 1976, **71**, 1196–1205.
31. Keays, R. R., Ross, J. R. and Woolrich, P. W., Precious metals in volcanic peridotite-associated nickel sulphide deposits in Western Australia. Part II: Distribution within the ores and host rocks at Kambalda. *Econ. Geol.*, 1981, **76**, 1645–1676.
32. Hoatson, D. M. and Keays, R. R., Formation of platiniferous sulphide horizons by crystal fractionation and magma mixing in the Munni Munni layered intrusion, West Pilbara Block, West Australia. *Econ. Geol.*, 1989, **84**, 1775–1804.
33. Vogel, D. C. and Keays, R. R., The petrogenesis and platinum-group element geochemistry of the Newer Volcanic Province, Victoria, Australia. *Chem. Geol.*, 1997, **136**, 181–204.
34. Ross, J. R. and Keays, R. R., Precious metals in volcanic-type nickel sulphide deposits in Western Australia I. Relationship with the composition of the ores and their host rocks. *Can. Mineral.*, 1979, **17**, 417–435.
35. Satyanarayanan, M., Balaram, V., Roy, P., Anjaiah, K. V. and Singh, S. P., Trace, REE and PGE geochemistry of the mafic and ultramafic rocks from Bundelkhand craton, central India. In *Advances in Geosciences* (ed. Satake, K.), 2010, vol. 20, pp. 57–80.

ACKNOWLEDGEMENTS. S.P.S. thanks Ministry of Mines for providing financial support. We are grateful to the Director, National Geophysical Research Institute, Hyderabad, for his support and permission to publish this paper. We also thank Prof. A. K. Basu and Dr M. E. A. Mondal for critically going through the initial draft of this manuscript.

Received 19 March 2009; revised accepted 28 June 2010